

PointLoc: Deep Pose Regressor for LiDAR Point Cloud Localization

Wei Wang¹, Bing Wang¹, Peijun Zhao¹, Changhao Chen¹, Ronald Clark²,
Bo Yang¹, Andrew Markham¹, and Niki Trigoni¹

Abstract—In this paper, we present a novel end-to-end learning-based LiDAR relocalization framework, termed PointLoc, which infers 6-DoF poses directly using only a single point cloud as input, without requiring a pre-built map. Compared to RGB image-based relocalization, LiDAR frames can provide rich and robust geometric information about a scene. However, LiDAR point clouds are sparse and unstructured making it difficult to apply traditional deep learning regression models for this task. We address this issue by proposing a novel PointNet-style architecture with self-attention to efficiently estimate 6-DoF poses from 360° LiDAR input frames. Extensive experiments on recently released challenging Oxford Radar RobotCar dataset and real-world robot experiments demonstrate that the proposed method can achieve accurate relocalization performance. We show that our approach improves the state-of-the-art MapNet by 69.59% in translation and 75.70% in rotation, and AtLoc by 66.86% in translation and 78.83% in rotation on the challenging outdoor large-scale Oxford Radar RobotCar dataset.

I. INTRODUCTION

LiDAR-based relocalization methods have achieved impressive accuracy [13], [15], [17]. A typical LiDAR relocalization system usually includes a feature extraction module, a feature matching algorithm, an outlier rejection step, a matching cost function, a spatial searching or optimization method and a temporal optimization or filtering mechanism [22]. Although these geometric localization methods achieve high accuracy in some scenarios, they require significant hand-engineering efforts to tune the huge amount of hyper-parameters, and depend heavily on the running environments. Therefore, these approaches are not scalable and difficult to be deployed in the real world.

A number of novel map-based approaches have been proposed to estimate global poses [2], [5], [19], [22], [35], [39]. For example, Barsan and Wang *et al.* [2] proposed to learn descriptors from LiDAR intensity, and relocalization was performed by matching descriptors against pre-built intensity maps. However, although these methods achieve considerable accuracy, it is hard to build the map and the computing complexity increases greatly when the map gets larger. Additionally, they require other systems to provide an accurate initial pose as coarse localization first.

Thus, most localization solutions employ Global Navigation Satellite System (GNSS) to provide pose estimations.

¹The authors are with the Department of Computer Science, University of Oxford, OX1 3QD, United Kingdom. {firstname.lastname}@cs.ox.ac.uk

²Ronald Clark is with the Department of Computing, Imperial College London, SW7 2AZ, United Kingdom. ronald.clark@imperial.ac.uk

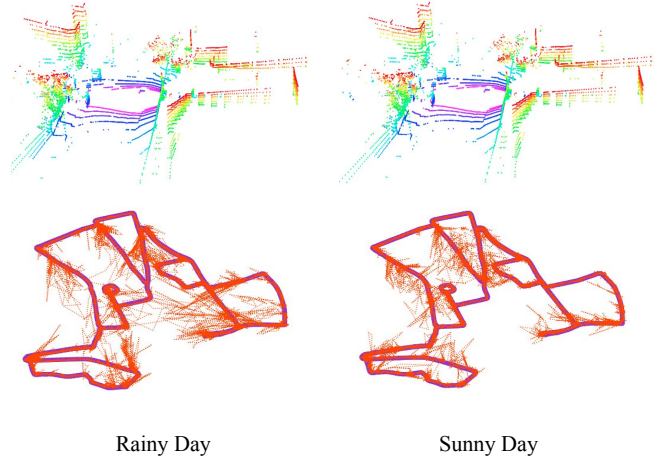


Fig. 1: PointLoc results for the challenging Oxford Radar RobotCar dataset [1], [23]. We directly feed the LiDAR point cloud from a single timestamp to the neural network for predicting the 6-DoF pose without the requirement of pre-built maps. The estimations of PointLoc are robust regardless of weather, and outperform the state-of-the-art DNN-based visual relocalization methods significantly.

Unfortunately, GNSS is not always available such as in indoor environments and the accuracy of GNSS cannot be guaranteed in areas like large cities where high-rising buildings can block the GNSS signals. To this end, Uy *et al.* [31] propose a point cloud retrieval-based localization method to deal with the situation when the GNSS is absent. It obtains a 6-DoF pose with respect to the pre-built map in the form of reference database. However, retrieval-based approaches inherently suffer from several issues. First, the time complexity of finding the closest match between the query point cloud and the reference point cloud is $O(n)$, which is not suitable for common real-time application scenarios. Second, the point cloud-based method requires a reference database, which occupies $O(n)$ storage space and cannot be deployed on many mobile robots. Third, the recall rate of it is often not good enough [31].

Recently, learning-based approaches have emerged as a promising tool to build up a completely end-to-end localization system. These methods not require any reference databases during runtime, and the learned features tend to be general and robust. These kind of localization approaches train a neural network to directly predict the pose. Their time complexity during inference time is $O(1)$ and the space it occupies is only the model size, which addresses the

drawbacks of point cloud retrieval-based methods. Early attempts in this direction include PoseNet and its variations [6], [11], [12], [30]. However, all the current pose regression approaches utilize RGB images as inputs, which have several problems. Visual inputs are sensitive to the change of environments, resulting in suboptimal localization performance. In addition, the input images are restricted to a narrow Field-of-View (FoV). These aspects restrict the application of these approaches to the real world. Compared with RGB images, point clouds, acquired by LiDAR, capture 360° 3-D space, and provide much richer geometric information of a specific location. In addition, the features extracted from point clouds tend to be more robust compared to those extracted from images. However, point clouds are sparse and unstructured, making it difficult to learn features for localization. Motivated by this, we design a neural network to use LiDAR point clouds as input for robust and accurate localization.

In this paper, we propose a novel neural network-based 3-D pose regressor, named PointLoc, to accurately estimate the 6-DoF pose using LiDAR point clouds. The neural network directly takes a primitive point cloud as input and estimates the 6-DoF pose in an end-to-end fashion. The performance shows significant improvement over the learning-based camera relocalization and LiDAR point cloud retrieval-based methods. Fig. 1 illustrates the superior performance of our PointLoc approach in different environments found in the Oxford Radar RobotCar dataset.

In summary, our contributions are as follows:

- To the best of our knowledge, this is the first LiDAR point cloud-based approach for deep pose regression. We demonstrate that the LiDAR relocalization problem can be solved in an end-to-end fashion by a point-based neural network. In addition, our proposed architecture with a self-attention module can further improve the accuracy of the predicted 6-DoF absolute poses.
- We conduct real-world robot experiments in an indoor environment. We will release the collected indoor LiDAR-image dataset dubbed vReLoc for studying the indoor relocalization task.
- Comprehensive experiments and an ablation study on these two new datasets have been done to evaluate our proposed method. Results demonstrate that the PointLoc model outperforms the state-of-the-art DNN-based visual relocalization and point cloud retrieval-based methods by a large margin.

II. RELATED WORKS

In this section, we first review different learning-based approaches for relocalization and then discuss some point cloud-based neural networks.

A. Learning to Localize

For dealing with the drawbacks of map registration methods, recent works propose learning-based approaches to estimate the global pose directly [3], [6], [8], [9], [11], [12], [24], [25], [29], [32], [34], [40]. They take images, either

single or sequential, as inputs to train a neural network model for predicting absolute poses. The key to these methods is to learn a deep pose regressor, which usually comprises a feature extractor and a regressor [9], [12], [36]. For example, PoseNet related works [10]–[12] proved the feasibility of predicting the global pose using a single RGB image by regressing the pose directly. Brahmabhatt *et al.* [3] utilized the relative pose between two images as a geometric constraint to estimate the pose. Huang *et al.* [9] and Wang *et al.* [36] have demonstrated that self-attention modules can significantly improve the accuracy of relocalization and guide the network to ignore distracting information from foreground objects in a dynamic environment. Although DNN-based relocalization methods can solve the downsides of retrieval-based approaches, the performance of translation and rotation estimation is still not satisfactory enough to be applied to real-world scenarios [30], which calls for further work on learning algorithms. Our work follows this line of study, aiming to improve the accuracy of deep pose regression.

B. Deep Learning on Point Clouds

DNN-based feature extraction methods for point clouds [16], [18], [26]–[28] have gained significant success in recent years. VoxelNet [43] was developed to learn feature embeddings in voxels for object detection. PointNet++ related works [26]–[28] have been proposed to directly process unordered point sets and learn features from points, which showed impressive performance on tasks of 3-D object detection, part segmentation, and semantic segmentation. Detailed introductions and applications of deep learning for point clouds can be found in the recent survey paper [20].

III. PROBLEM STATEMENT

We design a DNN-based framework for performing deep pose regression using point cloud data from a LiDAR sensor. We predict the absolute 6-DoF poses of the mobile agent within previously visited areas. A typical use case for our method would be when a mobile agent has already visited the query places before, and then has to localize itself again when it moves across the previously-visited environment. To enable a more generic and reliable relocalization system, we only consider one LiDAR input at a single timestamp rather than sequential inputs.

For each timestamp t , the agent receives one point cloud frame $\mathbf{P}_t = \{\mathbf{x}_i \mid i = 1, \dots, N\}$ from LiDAR, where each point \mathbf{x}_i is a vector of describing its coordinate (x, y, z) . Therefore, the shape for each \mathbf{P}_t is $(N, 3)$. The relocalization of the agent is parameterized by a 6-DoF pose $[\mathbf{t}, \mathbf{r}]^T$ with respect to the world coordinate, where $\mathbf{t} \in \mathbb{R}^3$ is a 3-D translation vector and $\mathbf{r} \in \mathbb{R}^4$ is a 4-D rotation vector (quaternion). To this end, deep 3-D pose regressors learn a function \mathcal{F} such that $\mathcal{F}(\mathbf{P}_t) = (\mathbf{t}, \mathbf{r})^T$, where the function \mathcal{F} is usually a neural network for DNN-based methods.

IV. DEEP POINT CLOUD RELOCALIZATION

This section introduces our proposed PointLoc, a deep 3-D pose regressor for predicting the global pose from point

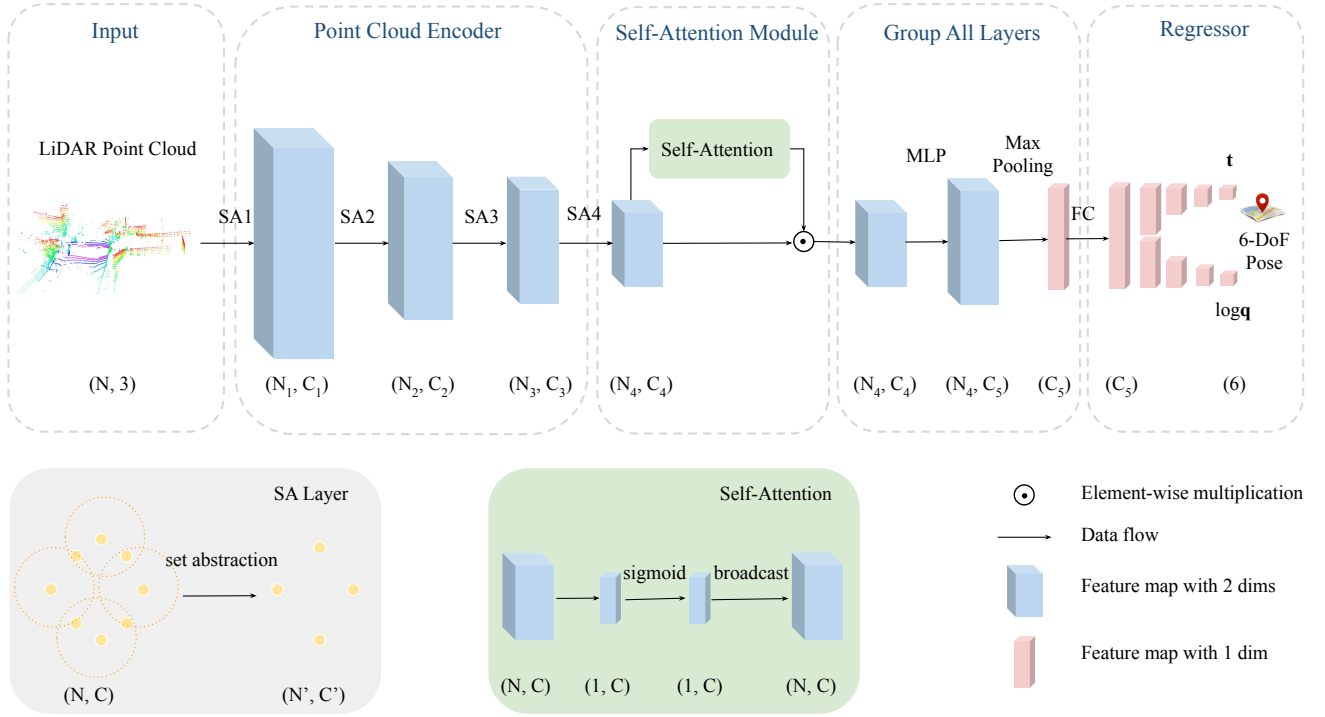


Fig. 2: The architecture of PointLoc. It consists of a point cloud encoder, a self-attention module, a grouping all (GA) layers module and a pose regressor. The encoder is composed of 4 consecutive set abstraction (SA) layers. Each SA layer shown in the diagram [21] consists of a sampling layer, a grouping layer and a PointNet layer [27]. The learnt point features are sent to self-attention module for eliminating the noisy features. Afterwards, these features are fed into group all (GA) layers for down-sampling to a feature vector. Finally, the pose regressor takes the feature vector as input and then regresses the 6-DoF Pose.

cloud data. The overall architecture is illustrated in Fig. 2. Our model consists of a point cloud encoder, a self-attention module, group all layers, and a pose regressor. The point cloud data are down-sampled to a fixed shape $(N, 3)$ as an input. The whole design is based on the PointNet-style structure, which can theoretically learn a critical subset of points for relocalization.

A. Point Cloud Pre-Processing

Each point cloud frame of a LiDAR scan contains a different number of points. However, our neural network requires the same point cloud dimensions $(N, 3)$ for its inputs. To tackle this problem, we adopt the random point cloud sampling strategy. We ensure that all the point cloud inputs have the same shape $(N, 3)$. N is set to 20,480 in this work.

B. Point Cloud Feature Encoder

The feature representation extracted by the point cloud encoder plays a critical role in achieving accurate and reliable relocalization. Intuitively, human beings can utilize key points and features in a scene to identify where they are and conventional geometric methods are capable of performing precise localization by exploiting key points of the point cloud data. Inspired by this, if a neural network learns a

subset of key points from the original point cloud data relevant to the localization task, we can take better advantage of these key features to identify a location. Existing literature [27], [42] has proved the critical-subset theory, i.e. for any point cloud \mathbf{P} , a PointNet-like structure can identify a salient point subset $\mathbf{C} \subseteq \mathbf{P}$, making it a desirable choice for our relocalization task.

Specifically, PointNet exploits the multi-layer perceptron (MLP), feature transformation module, and max pooling layer to approximate a permutation invariant function for point cloud classification and segmentation. In fact, it is a universal continuous set function approximator, described as:

$$f(x_1, \dots, x_N) = \phi(\mathbf{MAX}\{h(x_i) \mid x_i \in \mathbf{P}\}) \quad (1)$$

where ϕ and h are two continuous functions (they are usually instantiated to be an MLP), and \mathbf{MAX} denotes the max pooling layer [28]. PointNet++ extends PointNet by recursively capturing the hierarchical features on point sets in a metric space [28]. From the aforementioned Eq. 1, the result of the PointNet structure is determined by $u = \mathbf{MAX}\{h(x_i) \mid x_i \in \mathbf{P}\}$, and the \mathbf{MAX} operation takes N vectors as input and outputs one vector of element-wise maximums. Thus, there exists one $x_i \in \mathbf{P}$ such that $u_j = h_j(x_i)$, where u_j is the j^{th} dimension of u , and μ_j is the j^{th} dimension of $h(x_i)$. These points can be aggregated into

a critical subset $\mathbf{C} \subseteq \mathbf{P}$, where \mathbf{C} determines u and then $\phi(u)$ (more details can be found in [27], [42]). Consequently, the critical-subset theory is applicable to neural networks of the structure of $\phi(\mathbf{MAX}\{h(x_i) \mid x_i \in \mathbf{P}\})$. The proposed PointLoc is built upon PointNet++, consisting of such a structure and thus can learn the critical subset from LiDAR point clouds in theory.

C. Self-Attention for Robust Relocalization

Prior works [9], [36] have proved that the self-attention mechanism can improve camera relocalization by removing noisy features. Therefore, we also design a neural module to automatically remove the dynamic features before regressing the final poses. Inspired by the recent works [9], [36], [41], we introduce a simple self-attention module to learn a mask.

Given a set of point features $\mathbf{F} \in \mathbb{R}^{N \times C}$ which are learned from the point cloud encoder, our attention module aims to learn a mask $M \in \mathbb{R}^{1 \times C}$ for the features \mathbf{F} . To achieve this, we use a shared MLP followed by a *sigmoid* function to take the features \mathbf{F} as input and then directly generate the mask M . After that, we broadcast and mask the features \mathbf{F} by M , obtaining weighted features $\hat{\mathbf{F}}$ for subsequent pose regression. Formally, this self-attention module is defined as follows:

$$\hat{\mathbf{F}} = \mathbf{F} \cdot M \quad (2)$$

D. The Architecture of PointLoc

Accurate relocalization requires scene perception and geometric reasoning. The proposed PointLoc consists of a point cloud encoder, a self-attention module, grouping all (GA) layers and a pose regressor as shown in Fig. 2. Instead of extracting point cloud features by hand-crafted methods, we designed a point cloud encoder based on the set abstraction (SA) layer of PointNet++ [26], [28] as discussed before. The point cloud encoder is composed of 4 consecutive SA layers. Each SA layer is composed of a sampling layer, a grouping layer and a PointNet layer [27]. The SA layer takes a feature matrix $\mathbf{F} \in \mathbb{R}^{N \times C}$ as input where N is the point number and C is the feature dimension of each point, and outputs a feature matrix $\mathbf{F}' \in \mathbb{R}^{N' \times C'}$ where N' is the sub-sampled point number and C' is the new feature dimension of each point (from the size (N_1, C_1) to (N_4, C_4) in Fig. 2). We also leverage multi-scale grouping strategy [28] inside the SA layer for robust feature learning. Specifically, the layer adopts farthest point sampling to sample N' regions with x_j being the region centers, and for each region with radius r , it extracts local features with a symmetric function as [21]:

$$\mathbf{F}'_j = \mathbf{MAX}_{\{i \mid \|x_i - x_j\| \leq r\}} \{h(\mathbf{F}_i, x_i - x_j)\} \quad (3)$$

where \mathbf{F}_i is the i^{th} row of \mathbf{F} , \mathbf{F}'_j is the j^{th} row of \mathbf{F}' , $h: \mathbb{R}^C \rightarrow \mathbb{R}^{C'}$ is the MLP, and \mathbf{MAX} is the max pooling layer. After the last SA layer of the point cloud encoder, we apply a point self-attention module, which intends to learn a probability distribution to filter out features from outliers for better relocalization performance. Afterwards, the GA layer aggregates point features from all previous layers to

generate an embedded feature vector. Specifically, shown in Fig. 2, the input of the GA layer is a point feature set of size $N_4 \times C_4$, and then the point features are propagated to an updated point feature set of size $N_4 \times C_5$ via MLP, where C_5 is larger than C_4 . Next, it is down-sampled to the C_5 dimension feature vector through the max pooling layer. The embedded feature vector is then forwarded to an FC layer. After the FC layer, the C_5 dimensional feature vector is finally sent to the pose regressor for predicting the translation \mathbf{t} and rotation \mathbf{r} respectively. The pose regressor is composed of consecutive FC layers.

E. Loss Function

Our goal is to estimate the 6-DoF pose $[\mathbf{t}, \mathbf{r}]^T$. Prior works [6], [7], [11], [12] directly predict quaternions and use an l_1 or l_2 loss, but such a representation is over-parameterized and normalization of the output quaternion is required at the cost of worse accuracy [3]. Odometry tasks with DNNs [37], [38] usually regress Euler angles, which are also not suitable here since they wrap around 2π . Consequently, we employ the definition of the loss function in [3] for training our neural network, which is adapted from [11]. Given training samples $\mathcal{G} = \{(\mathbf{P}_i, \mathbf{I}_i) \mid i = 1, \dots, N\}$ and their corresponding ground-truth poses $\{[\hat{\mathbf{t}}, \hat{\mathbf{r}}]_i^T \mid i = 1, \dots, N\}$, the parameters of the PointLoc are learned via the following loss function:

$$\mathcal{L}(\mathcal{G}) = \|\mathbf{t} - \hat{\mathbf{t}}\|_1 e^{-\beta} + \beta + \|\log \mathbf{q} - \log \hat{\mathbf{q}}\|_1 e^{-\gamma} + \gamma \quad (4)$$

where β and γ are balanced factors to jointly learn translation and rotation. It is worth noting that the β and γ are learnable factors during training, which are initialized by β^0 and γ^0 respectively. $\log \mathbf{q}$ is the logarithmic form of a unit quaternion $\mathbf{q} = (u, \mathbf{v})$, where u is a scalar and \mathbf{v} is a 3-D vector. It is defined as:

$$\log \mathbf{q} = \begin{cases} \frac{\mathbf{v}}{\|\mathbf{v}\|} \cos^{-1} u, & \text{if } \|\mathbf{v}\| \neq 0 \\ \mathbf{0}, & \text{otherwise} \end{cases} \quad (5)$$

V. INDOOR LiDAR RELOCALIZATION DATASET

There is a lack of public datasets in the indoor environment with point cloud data. In order to boost the research in this area, we collected a new dataset dubbed vReLoc with rich sensor modalities, e.g. vision and LiDAR data on a mobile robot platform. Our dataset will be released to benefit future researchers.

The experimental robot is Turtlebot 2, mounted with a Velodyne HDL-32E LiDAR and an Intel RealSense Depth Camera D435. The sensors have been carefully calibrated. The Velodyne is a lightweight pulsed laser for Detection and Ranging, which features 32 lasers across over a 40° vertical field-of-view and a 360° horizontal field-of-view. It runs at a frequency of 10Hz. Each point cloud in the dataset contains $\sim 60,000$ points. The camera was employed to capture RGB images, and the size of each image is $640 \times 480 \times 3$. A Vicon Motion Tracker system is leveraged for acquiring accurate ground truth 6-DoF poses. 10 Bonita B10 cameras are used in the system, installed around the area where the dataset is collected. Each Bonita B10 has the resolution of 1 megapixel

TABLE I: Dataset Descriptions on the vReLoc.

Sequence	Scenario	Training	Test
Seq-03	static	✓	
Seq-12, Seq-15	one-person walking	✓	
Seq-16	two-persons walking	✓	
Seq-05, Seq-06, Seq-07	static		✓
Seq-14	one-person walking		✓

with 250 fps frame rate, and an operating range of up to 13 m. The system can track the pose of the robot at a precision of ~ 1 cm.

The size of the Vicon room is about $4m \times 5m$. We lay out several obstacles in the scene. For the relocalization task, the scene is fixed through the whole data collection process. We utilized the Robot Operating System (ROS) for robot control and data collection. Timestamps were recorded on every frame of each sensor by the ROS, and we synchronized world timestamp across different systems from the same Network Time Protocol (NTP) server.

A total of 18 sequences were collected of various lengths. Since the Velodyne LiDAR, RealSensor camera and Vicon motion tracker system run in different frequencies, we synchronized these systems so that the image and LiDAR in each timestamp has the same 6-DoF pose. For the static scenario, there are no moving objects in the scene. For other scenarios, there are people randomly walking in the scene. Sequences 01-10 come from the static environment, sequences 11-15 are the one-person moving scenario, and sequences 16-18 are two-persons moving scenario. In order to better represent real-world situations, in our experiments, we specially chose challenging sequences as the training dataset. We report our training and test sequences from the vReLoc dataset in Table I.

VI. EXPERIMENTS

In this section, we evaluate our proposed approach on the recently released outdoor Oxford Radar RobotCar [1], [23] dataset and our proposed indoor vReLoc dataset and compare to state-of-the-art methods.

A. Implementation Details

Adam [14] is applied to train our network with $\beta_1 = 0.9$ and $\beta_2 = 0.999$. We set the initial values $\beta_0 = 0.0$ and $\gamma_0 = -3.0$ of the loss function. The learning rate is set to 0.001, and we train 100 epochs on both datasets. For baseline image approaches, we also used data augmentation to improve the accuracy of predictions. Following the convention of existing works [4], [11], [12], [30], [36], we calculate the mean error for outdoor datasets and the median error for indoor datasets.

The parameter settings of the point cloud encoder is shown in Table II. In Table III, we present the parameter settings of the self-attention module. The parameter setting of the group all layers is shown in Table IV. We show the parameter setting of the pose regressor in Table V.

TABLE II: Parameter Setting of the Point Cloud Encoder.

Layer Name	Point Num	Radius	Sample Num	MLP
SA1	2048	0.2	64	[0, 64, 64, 128]
SA2	1024	0.4	32	[128, 128, 128, 256]
SA3	512	0.8	16	[256, 128, 128, 256]
SA4	256	1.2	16	[256, 128, 128, 256]

TABLE III: Parameter Setting of the Self-Attention Module.

Layer Name	Point Dimension	Feature Dimension
Self-Attention Module	256	256

TABLE IV: Parameter Setting of the Group All Layers.

Layer Name (Ignore Max Pooling Layer)	Feature Dimension
Multi-Layer Perceptron (MLP)	[256, 256, 512, 1024]
Fully-Connected Layer (FC)	1024

TABLE V: Parameter Setting of the Pose Regressor. \mathbf{t} branch and $\log \mathbf{q}$ branch share the same parameter setting.

Layer Name	Feature Dimension	LeakyReLU
FC1 + LeakyReLU	[1024, 512]	0.2
FC2 + LeakyReLU	[512, 128]	0.2
FC3 + LeakyReLU	[128, 64]	0.2
FC4	[64, 3]	NA

B. Baselines

To validate the performance of the proposed PointLoc, we compare it with several state-of-the-art learning-based camera relocalization approaches as well as point cloud retrieval-based approaches. Since the Radar RobotCar dataset does not have depth images and the projection of the LiDAR point cloud is too sparse, we compare PointLoc with RGB-based camera relocalization methods. Considering that the LiDAR can provide depth information, for a fair comparison, in our vReLoc dataset, we collected depth images, and used the late fusion strategy to fuse RGB and depth images for comparison. For these two datasets, we choose PoseNet17 [11] as the baseline since it outperforms PoseNet and Bayesian PoseNet in previous works. AtLoc [36] is selected for comparison since it is the state-of-the-art single image-based learning approach. We also choose LSTM-Pose [34] as the sequential baseline. Moreover, we also compare with MapNet [4] because it is the state-of-the-art sequential image approach. We note that sequential methods generally perform better than single image ones by utilizing time constraints. However, for the relocalization task, this past information is not always available as discussed before. We still compare with them to examine how competitive our method is. For large-scale point cloud relocalization methods, we compare with PointNetVLAD. We create the triplet training dataset, increase the point number from 4,096 to 8,192, and set the loss margin from 0.5 to 1.0 to improve the performance, while other hyper-parameters are kept the same as the vanilla PointNetVLAD. We note that we implement baseline

TABLE VI: Dataset Descriptions on the Oxford Radar RobotCar.

Scene	Time	Tag	Training	Validation	Test
FULL1	2019-01-11-14-02-26	sun	✓		
FULL2	2019-01-14-12-05-52	overcast	✓		
FULL3	2019-01-14-14-48-55	overcast	✓		
FULL4	2019-01-18-15-20-12	overcast	✓		
FULL5	2019-01-15-14-24-38	overcast		✓	
FULL6	2019-01-10-11-46-21	rain			✓
FULL7	2019-01-15-13-06-37	overcast			✓
FULL8	2019-01-17-14-03-00	sun			✓
FULL9	2019-01-18-14-14-42	overcast			✓

methods and tune them for the best performance.

C. Results on the Oxford Radar RobotCar

The Oxford Radar RobotCar dataset [1] is a radar extension to the Oxford RobotCar dataset [23], providing data from dual Velodyne HDL-32E LiDARs and Grasshopper2 monocular cameras. The ground truth poses are obtained by a NovAtel SPAN-CPT ALIGN inertial and GPS navigation system (GPS/INS).

Dataset Description The data were gathered in January 2019 over thirty-two traversals of a central Oxford route, and the duration and distance of each traversal are ~ 32 mins and ~ 9.05 km respectively. The resolution of a captured RGB image is 1280×960 , and each point cloud has $\sim 21,000$ points. We observe that the dataset is large-scale, covers various weather conditions and has moving objects like people and cars in the scenes, all of which have significant influence on the accuracy of relocalization task, and therefore it is quite challenging. Since there is a timestamp misalignment between camera and LiDAR sensors, we synchronize timestamps and interpolate (GPS/INS) measurements to coincide with the ground truth poses. We report the training and test sequences we used from the Oxford Radar RobotCar in Table VI.

Results The test results of the Radar RobotCar are presented in Table VII. Following the plotting style of relocalization work [9], the trajectories of FULL7 and FULL8 of LSTM-Pose, MapNet, AtLoc, and PointLoc are shown in Fig. 3. The proposed PointLoc consistently outperforms the RGB learning-based camera relocalization baselines by a large margin. The results demonstrate that instead of utilizing RGB images as the sensory input, LiDAR point cloud can significantly improve the relocalization accuracy. Our pose predictions are even better than the sequential approaches like MapNet. In addition, the variance of learning-based camera relocalization is much larger than our approach. Therefore, PointLoc can have stable estimation across the test dataset, which indicates that the point cloud relocalization method is more robust than the visual relocalization. Furthermore, PointLoc is much better than the LiDAR point cloud retrieval-based approach PointNetVLAD in terms of accuracy, which proves the effectiveness of our proposed network. As seen from Table VIII, PointLoc can satisfy real-time operation and the storage space is small. This indicates that PointLoc is better than existing point cloud retrieval-based approaches for relocalization.

TABLE VII: Mean translation error (m) and rotation error ($^\circ$) for the state-of-the-art methods on the Oxford Radar RobotCar.

Scene	PoseNet17 [11]	LSTM-Pose [33]	MapNet [4]	AtLoc [36]	PointNetVLAD [31]	PointLoc (Ours)
FULL6	51.05m, 6.41 $^\circ$	38.47m, 5.36 $^\circ$	32.16m, 5.40 $^\circ$	28.57m, 7.99 $^\circ$	28.48m, 5.19 $^\circ$	13.81m, 1.53$^\circ$
FULL7	80.29m, 6.51 $^\circ$	54.59m, 4.56 $^\circ$	47.79m, 5.44 $^\circ$	36.86m, 5.17 $^\circ$	17.62m, 3.95 $^\circ$	9.81m, 1.27$^\circ$
FULL8	111.24m, 12.78 $^\circ$	77.57m, 9.74 $^\circ$	51.93m, 7.73 $^\circ$	58.63m, 8.53 $^\circ$	23.59m, 5.87 $^\circ$	11.51m, 1.34$^\circ$
FULL9	45.50m, 3.96 $^\circ$	26.16m, 2.56 $^\circ$	14.93m, 2.84 $^\circ$	10.67m, 2.88 $^\circ$	13.71m, 2.57 $^\circ$	9.51m, 1.07$^\circ$
Average	72.02m, 7.42 $^\circ$	49.20m, 5.49 $^\circ$	36.70m, 5.35 $^\circ$	33.68m, 6.14 $^\circ$	20.85m, 4.40 $^\circ$	11.16m, 1.30$^\circ$

TABLE VIII: Comparisons of the computational time and storage space of PointLoc and PointNetVLAD.

	Computational Time	Storage Space
PointLoc	0.0985 sec	13 MB
PointNetVLAD	38.0242 sec	283 MB (76 MB model size and 207 MB reference db size)

D. Results on a Real-World Indoor Robot

We also validate our proposed PointLoc on the real-world indoor robot dataset. Our experimental design simulates the real-world scenarios of robot movements like service robots inside a large shopping mall. The robot moved forward and backward, halting when it faces obstacles. Data was collected under three conditions: static environment, one-person walking, and two-persons walking. We named the collected dataset vReLoc since it was acquired in a Vicon room for indoor relocalization task. It includes in total 18 robot movement sequences in an indoor Vicon environment. vReLoc will be released to help support future work on relocalization.

We report our test results in Table IX. The trajectories of test results using our PointLoc are plotted in Fig. 4. The results show that PointLoc outperforms both the RGB and the RGB-D baselines in the indoor environment, which demonstrates that the proposed LiDAR relocalization is better for deep pose regression. Due to the broad geometric information provided by LiDAR, the rotation estimation is always better than other methods. Furthermore, by adding the depth image, the rotation performance of PoseNet17 and AtLoc is largely improved.

E. Ablation Study

To explore the impact of various components of our PointLoc, we conducted the following ablation studies. First, we replaced the point cloud encoder with PointNet. Our goal is to examine whether the PointNet++ based SA module is an effective point cloud feature learning architecture. Second, the self-attention module was removed from the architecture since we want to see whether the noisy point features can be eliminated. In Table X, we report results on the Oxford Radar RobotCar dataset.

The results of PointLoc outperform the PointNet encoder-based architecture, which suggests the effectiveness of hierarchical feature learning design, and the good performance of the PointNet encoder reveals that the PointNet-style architecture is helpful for the LiDAR relocalization task. Moreover, the self-attention module indeed enhances the accuracy of relocalization. We also observed that the self-attention mechanism did not improve the performance dramatically as it does in the visual relocalization. There

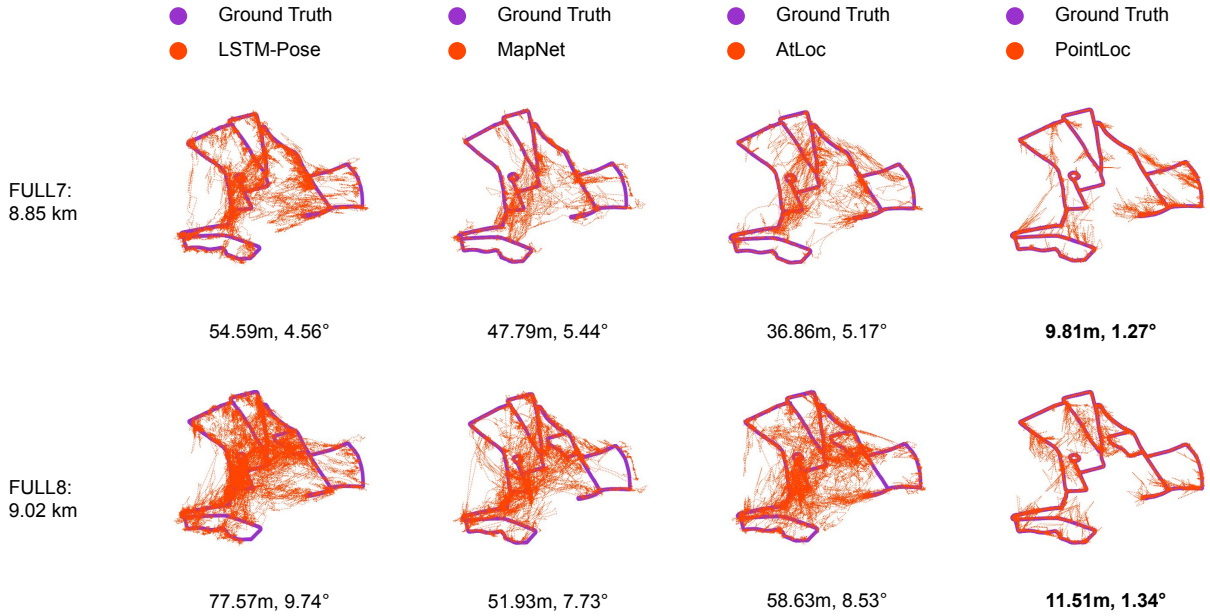


Fig. 3: Trajectories of LSTM-Pose, MapNet, AtLoc and the proposed PointLoc on FULL7 and FULL8 with mean translation error (m) and rotation error ($^{\circ}$). The darkorchid line is the ground truth poses, and the orange-red dot line shows the estimated poses. Our PointLoc outperforms the existing camera relocalization approaches by a significant margin.

TABLE IX: Median translation error (m) and rotation error ($^{\circ}$) for the state-of-the-art methods on the vReLoc dataset.

Scene	PoseNet17 [11]	PoseNet17 w/ RGB-D [11]	LSTM-Pose [33]	MapNet [4]	AtLoc [36]	AtLoc w/ RGB-D [36]	PointLoc (Ours)
Seq-05	0.20m, 4.58 $^{\circ}$	0.16m, 4.43 $^{\circ}$	0.19m, 4.21 $^{\circ}$	0.16m, 4.18 $^{\circ}$	0.17m, 3.59 $^{\circ}$	0.16m, 3.46 $^{\circ}$	0.12m, 3.00$^{\circ}$
Seq-06	0.18m, 5.13 $^{\circ}$	0.19m, 4.63 $^{\circ}$	0.17m, 4.71 $^{\circ}$	0.15m, 4.92 $^{\circ}$	0.16m, 6.45 $^{\circ}$	0.15m, 4.15 $^{\circ}$	0.10m, 2.97$^{\circ}$
Seq-07	0.22m, 5.24 $^{\circ}$	0.25m, 5.26 $^{\circ}$	0.19m, 4.08 $^{\circ}$	0.21m, 5.60 $^{\circ}$	0.21m, 8.25 $^{\circ}$	0.19m, 4.08 $^{\circ}$	0.13m, 3.47$^{\circ}$
Seq-14	0.12m, 5.36 $^{\circ}$	0.12m, 4.90 $^{\circ}$	0.11m, 2.88 $^{\circ}$	0.10m, 4.94$^{\circ}$	0.10m, 5.81$^{\circ}$	0.11m, 3.39 $^{\circ}$	0.11m, 2.84$^{\circ}$
Average	0.18m, 5.08 $^{\circ}$	0.18m, 4.81 $^{\circ}$	0.17m, 3.97 $^{\circ}$	0.16m, 4.91 $^{\circ}$	0.16m, 6.03 $^{\circ}$	0.15m, 3.77 $^{\circ}$	0.12m, 3.07$^{\circ}$

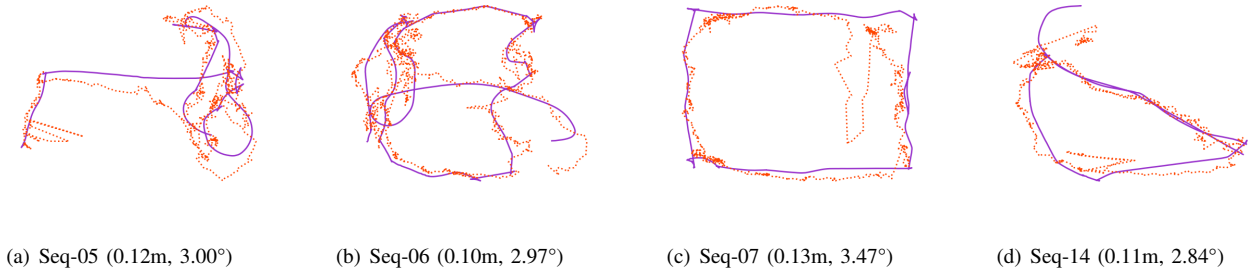


Fig. 4: Trajectories of the proposed PointLoc on the vReLoc test dataset with median translation error (m) and rotation error ($^{\circ}$). The darkorchid line is the ground truth poses, and the orange-red dot line is the estimated poses.

TABLE X: Ablation study on the Oxford Radar RobotCar.

Scene	PointNet Encoder	PointLoc w/o SA	PointLoc
FULL6	18.45m, 2.08 $^{\circ}$	15.24m, 1.95 $^{\circ}$	13.81m, 1.53 $^{\circ}$
FULL7	14.84m, 2.17 $^{\circ}$	11.32m, 1.72 $^{\circ}$	9.81m, 1.27 $^{\circ}$
FULL8	16.39m, 2.26 $^{\circ}$	13.63m, 1.80 $^{\circ}$	11.51m, 1.34 $^{\circ}$
FULL9	13.60m, 1.86 $^{\circ}$	11.03m, 1.41 $^{\circ}$	9.51m, 1.07 $^{\circ}$
Average	15.82m, 2.09 $^{\circ}$	12.10m, 1.62 $^{\circ}$	11.16m, 1.30 $^{\circ}$

may be two reasons. First, the designed architecture already has the ability to learn static key points. Second, other approaches need to be studied to remove the outlier features from the point cloud data.

VII. CONCLUSION

This paper presents a novel LiDAR relocalization approach, PointLoc, based on deep learning. Leveraging a

point-based neural network, it achieves superior relocalization accuracy compared to image-based and point cloud retrieval-based approaches. The approach can be applied to large-scale relocalization and robot navigation scenarios for meter-level localization requirements. It can also be leveraged in indoor environments or urban areas full of high-rise buildings as a complement when the GNSS is absent. For centimeter-level requirement scenarios like autonomous driving, it can serve as a coarse localization method to provide good initial pose estimates where point cloud registration and RANSAC can be applied to further improve the accuracy of relocalization. In the future, more explorations can be done for further improving the relocalization accuracy such as eliminating the noisy point features from the point cloud.

VIII. ACKNOWLEDGEMENT

This work is funded by the NIST grant 70NANB17H185. "Pervasive, Accurate, and Reliable Location-Based Services for Emergency Responders".

REFERENCES

- [1] D. Barnes, M. Gadd, P. Murcutt, P. Newman, and I. Posner. The Oxford Radar RobotCar Dataset: A Radar Extension to the Oxford RobotCar Dataset. *arXiv*, 2019.
- [2] I. A. Barsan, S. Wang, A. Pokrovsky, and R. Urtasun. Learning to Localize Using a LiDAR Intensity Map. *CoRL*, 2018.
- [3] S. Brahmabhatt, J. Gu, K. Kim, J. Hays, and J. Kautz. Geometry-Aware Learning of Maps for Camera Localization. *CVPR*, 2018.
- [4] S. Brahmabhatt, J. Gu, K. Kim, J. Hays, and J. Kautz. Geometry-Aware Learning of Maps for Camera Localization. *CVPR*, 2018.
- [5] F. Camposco, A. Cohen, M. Pollefeys, and T. Sattler. Hybrid Scene Compression for Visual Localization. *CVPR*, 2019.
- [6] R. Clark, S. Wang, A. Markham, N. Trigoni, and H. Wen. VidLoc: A deep spatio-temporal model for 6-DoF video-clip relocalization. *CVPR*, 2017.
- [7] R. Clark, S. Wang, H. Wen, A. Markham, and N. Trigoni. ViNet: Visual-Inertial Odometry as a Sequence-to-Sequence Learning Problem. *AAAI*, 2017.
- [8] Y. Feng, L. Ma, W. Liu, and J. Luo. Spatio-temporal Video Relocalization by Warp LSTM. *CVPR*, 2019.
- [9] Z. Huang, Y. Xu, J. Shi, and X. Zhou. Prior Guided Dropout for Robust Visual Localization in Dynamic Environments. *ICCV*, 2019.
- [10] A. Kendall and R. Cipolla. Modelling uncertainty in deep learning for camera relocalization. *ICRA*, 2016, 2016.
- [11] A. Kendall and R. Cipolla. Geometric Loss Functions for Camera Pose Regression with Deep Learning. *CVPR*, 2017.
- [12] A. Kendall, M. Grimes, and R. Cipolla. PoseNet: A Convolutional Network for Real-Time 6-DOF Camera Relocalization. *ICCV*, 2015.
- [13] H. Kim, B. Liu, C. Y. Goh, S. Lee, and H. Myung. Robust vehicle localization using entropy-weighted particle filter-based data fusion of vertical and road intensity information for a large scale urban area. *RA-L*, 2017.
- [14] D. P. Kingma and J. Ba. Adam: A Method for Stochastic Optimization. *ICLR*, 2015.
- [15] R. Kümmerle, D. Hähnel, D. Dolgov, S. Thrun, and W. Burgard. Autonomous driving in a multi-level parking structure. *ICRA*, 2009.
- [16] T. Le and Y. Duan. PointGrid: A Deep Network for 3D Shape Understanding. *CVPR*, 2018.
- [17] J. Levinson and S. Thrun. Robust Vehicle Localization in Urban Environments Using Probabilistic Maps. *ICRA*, 2010.
- [18] R. Li, S. Wang, Z. Long, and D. Gu. UnDeepVO: Monocular Visual Odometry through Unsupervised Deep Learning. *ICRA*, 2018.
- [19] L. Liu, H. Li, and Y. Dai. Efficient Global 2D-3D Matching for Camera Localization in a Large-Scale 3D Map. *ICCV*, 2017.
- [20] W. Liu, J. Sun, W. Li, T. Hu, and P. Wang. Deep learning on point clouds and its application: A survey. *Sensors*, 2019.
- [21] X. Liu, C. R. Qi, and L. J. Guibas. FlowNet3D : Learning Scene Flow in 3D Point Clouds. *CVPR*, 2019.
- [22] W. Lu, Y. Zhou, G. Wan, S. Hou, and S. Song. L3-Net : Towards Learning based LiDAR Localization for Autonomous Driving. *CVPR*, pages 6389–6398, 2019.
- [23] W. Maddern, G. Pascoe, C. Linegar, and P. Newman. 1 Year, 1000km: The Oxford RobotCar Dataset. *IJRR*, 2016.
- [24] I. Melekhov, J. Ylioinas, J. Kannala, and E. Rahtu. Image-Based Localization Using Hourglass Networks. *ICCV-W 2017*, 2017.
- [25] T. Naseer and W. Burgard. Deep regression for monocular camera-based 6-DoF global localization in outdoor environments. *IROS*, 2017.
- [26] C. R. Qi, O. Litany, K. He, and L. J. Guibas. Deep Hough Voting for 3D Object Detection in Point Clouds. *ICCV*, 2019.
- [27] C. R. Qi, H. Su, K. Mo, and L. J. Guibas. PointNet: Deep Learning on Point Sets for 3D Classification and Segmentation. *CVPR*, 2017.
- [28] C. R. Qi, L. Yi, H. Su, and L. J. Guibas. PointNet++: Deep Hierarchical Feature Learning on Point Sets in a Metric Space. *NeurIPS*, 2017.
- [29] N. Radwan, A. Valada, and W. Burgard. VLocNet++: Deep Multitask Learning for Semantic Visual Localization and Odometry. *IEEE Robotics and Automation Letters*, 3(4):4407–4414, 2018.
- [30] T. Sattler, Q. Zhou, M. Pollefeys, and L. Leal-taix. Understanding the Limitations of CNN-based Absolute Camera Pose Regression Chalmers University of Technology. *CVPR*, 2019.
- [31] M. A. Uy and G. H. Lee. PointNetVLAD: Deep Point Cloud Based Retrieval for Large-Scale Place Recognition. *CVPR*, 2018.
- [32] A. Valada, N. Radwan, and W. Burgard. Deep Auxiliary Learning for Visual Localization and Odometry. *ICRA*, 2018.
- [33] F. Walch, C. Hazirbas, L. Leal-Taixe, T. Sattler, S. Hilsenbeck, and D. Cremers. Image-Based Localization Using LSTMs for Structured Feature Correlation. *ICCV*, 2017.
- [34] F. Walch, C. H. L. Leal-taix, T. Sattler, and S. H. D. Cremers. Image-based localization using LSTMs for structured feature correlation. *ICCV*, 2017.
- [35] G. Wan, X. Yang, R. Cai, H. Li, Y. Zhou, H. Wang, and S. Song. Robust and Precise Vehicle Localization Based on Multi-Sensor Fusion in Diverse City Scenes. *ICRA*, pages 4670–4677, 2018.
- [36] B. Wang, C. Chen, C. X. Lu, P. Zhao, N. Trigoni, and A. Markham. AtLoc: Attention Guided Camera Localization. *AAAI*, 2020.
- [37] S. Wang, R. Clark, H. Wen, and N. Trigoni. DeepVO: Towards End-to-End Visual Odometry with Deep Recurrent Convolutional Neural Networks. *ICRA*, 2017.
- [38] W. Wang, M. R. U. Saputra, P. Zhao, P. Gusmao, B. Yang, C. Chen, A. Markham, and N. Trigoni. DeepPCO : End-to-End Point Cloud Odometry through Deep Parallel Neural Network. *IROS*, 2019.
- [39] X. Wei, I. A. Barsan, S. Wang, J. Martinez, and R. Urtasun. Learning to Localize Through Compressed Binary Maps. *CVPR*, 2019.
- [40] F. Xue, X. Wang, Z. Yan, Q. Wang, J. Wang, and H. Zha. Local Supports Global: Deep Camera Relocalization with Sequence Enhancement. *ICCV*, 2019.
- [41] B. Yang, S. Wang, A. Markham, and N. Trigoni. Robust Attentional Aggregation of Deep Feature Sets for Multi-view 3D Reconstruction. *IJCV*, 2019.
- [42] T. Zheng, C. Chen, J. Yuan, B. Li, and K. Ren. PointCloud Saliency Maps. *ICCV*, 2019.
- [43] Y. Zhou and O. Tuzel. VoxelNet: End-to-End Learning for Point Cloud Based 3D Object Detection. *CVPR*, 2018.